PNAS RESEARCH ARTICLE | APPLIED PHYSICAL SCIENCES

Hopping and crawling DNA-coated colloids

Jeana Aojie Zheng[a], Miranda Holmes-Cerfon[b], David J. Pine[a,c], and Sophie Marbach[d,e,1]

Affiliations are included on p. 9.

Edited by Noel Clark, University of Colorado Boulder, Boulder, CO; received October 28, 2023; accepted August 9, 2024

Understanding the motion of particles with multivalent ligand-receptors is important for biomedical applications and material design. Yet, even among a single design, the prototypical DNA-coated colloids, seemingly similar micrometric particles hop or roll, depending on the study. We shed light on this problem by observing DNA-coated colloids diffusing near surfaces coated with complementary strands for a wide array of coating designs. We find colloids rapidly switch between 2 modes: They hop—with long and fast steps—and crawl—with short and slow steps. Both modes occur at all temperatures around the melting point and over various designs. The particles become increasingly subdiffusive as temperature decreases, in line with subsequent velocity steps becoming increasingly anticorrelated, corresponding to switchbacks in the trajectories. Overall, crawling (or hopping) phases are more predominant at low (or high) temperatures; crawling is also more efficient at low temperatures than hopping to cover large distances. We rationalize this behavior within a simple model: At lower temperatures, the number of bound strands increases, and detachment of all bonds is unlikely, hence, hopping is prevented and crawling favored. We thus reveal the mechanism behind a common design rule relying on increased strand density for long-range self-assembly: Dense strands on surfaces are required to enable crawling, possibly facilitating particle rearrangements.

diffusion | colloids | DNA | multivalent ligand–receptors | subdiffusion

Significance

Understanding how "sticky" particles move and interact with their environment has broad implications, from biomedical targeting and screening to designing innovative materials. These micrometric particles possess "molecular stickers" constantly binding and unbinding to other surfaces. At the macroscopic scale, they appear to hop, roll, or crawl, yet experimental microscopic understanding remains elusive. Using DNA-coated particles as an experimental model, our research reveals a fascinating duality: These particles alternate between hopping and crawling on surfaces, with temperature playing a crucial role. They prefer hopping with long steps at higher temperatures, while they crawl with short steps at lower temperatures. We build a model attributing this behavior to an increased sticker strength at lower temperatures, preventing bond detachment and hopping.

Understanding the motion of particles with multivalent ligand-receptors is of broad interest for applications ranging from biomedical targeting (1–5) and screening (6, 7) to material design (8, 9) and water pollution remediation (10). Such particles, a few nanometers to several microns in size, rely on specific binding and unbinding of up to thousands of fluctuating ligands—or feet—to stick to receptor-coated surfaces. Such ligand–receptor interactions also affect how the particles move in ways that can be essential for their function. A prototypical example is DNA-coated colloids (9), which use DNA hybridization as the ligand–receptor bond that tethers colloids and mediates the self-assembly (11, 12), in large-scale colloidal crystals (13–20) or reconfigurable colloidal molecules (8, 21, 22).

Self-assembly and material design with DNA-coated colloids strongly depend not only on the binding strength but also on kinetic pathways (20) and especially on the relative motion of the DNA-coated colloids: If the bonds are too sticky, relative motion is limited, which prohibits particle rearrangements (23, 24). Several recent models have suggested ways to enhance diffusion with local bond resetting (25) or by adapting the relative bond strength (26, 27). This demonstrates the critical need to understand the mechanisms governing the relative motion of such DNA-coated surfaces to guide design strategies for improved assembly kinetics.

Nevertheless, a mechanistic understanding of the relative motion of such particles is still lacking. This is because of the complex, multiscale nature of the motion, with fast, small-scale, experimentally unresolvable ligand–receptor bonding dynamics giving rise to relative motion on the macroscale. This motion can take a variety of forms: Ligand–receptor particles can hop, roll, slide, crawl, glide, or remain trapped (23, 28–36), depending on the microscopic bonding conditions. Even for a single well-defined system, the preferred mode of motion can vary: Micron-sized DNA-coated colloids at equilibrium with similar coatings were seen to mostly hop (28) or to perform cohesive moves (30), to diffuse (37–39), or to subdiffuse (28, 30). The multiscale nature of the motion challenges theoretical work (26, 34, 37, 40–46), calling for high-throughput experiments.

In this work, we experimentally demonstrate that micron-sized colloids move along a DNA-coated surface, randomly alternating between two mobility modes: hopping, characterized by long steps in each resolvable time interval, and crawling, characterized by short steps. This gives rise to a step-size distribution that is distinctly non-Gaussian,

Author contributions: M.H.-C., D.J.P., and S.M. designed research; J.A.Z. and S.M. performed research; J.A.Z. and S.M. analyzed data; and J.A.Z., M.H.-C., D.J.P., and S.M. wrote the paper.

The authors declare no competing interest.

This article is a PNAS Direct Submission.

[1]To whom correspondence may be addressed. Email: sophie.marbach@cnrs.fr.

This article contains supporting information online at https://www.pnas.org/lookup/suppl/doi:10.1073/pnas.2318865121/-/DCSupplemental.

Published October 1, 2024.

both in single-particle trajectories and at the ensemble level, and well-modeled by a sum of two Gaussians with different widths. Both modes of motion are present over a range of temperatures spanning the melting point of the system, but hopping contributes the most to the mean-squared displacement of the particles at high temperatures, while crawling contributes the most at low temperatures. We build a theoretical model that reproduces most of the experimental features and brings mechanistic insight: At high temperatures, the number of bonds with the surface is small enough to permit coordinated detachment of all bonds, followed by free diffusion, then reattachment, corresponding to the long steps observed in the hopping mode. At lower temperatures, the number of bonds increases and a cohesive motion mode dominates. This latter mode could correspond to any cohesive motion (rolling, sliding, antirolling, rocking around the tethering point or combinations of all of these), which we collectively refer to as crawling. Finally, we shed light on the mechanism yielding subdiffusion at low temperatures: Trajectories tend to reverse back on themselves, resulting in anticorrelated motion determining the subdiffusive exponent. Unraveling how mobility depends on experimental parameters such as coating densities and temperature paves the way toward rational programming of ligand–receptor-mediated processes.

DNA-Coated Colloids Hop and Crawl at the Single Particle Level. We track with an optical microscope the motion of 800 DNA-coated colloids, $R = 500$ nm in radius, as they diffuse on a DNA-coated substrate (Fig. 1*A*). Our fabrication procedure is similar to previous work (47, 48) (*SI Appendix*, section 1). Briefly, on the polystyrene particle, single-stranded DNA is anchored through a polyethylene oxide (PEO) linker using click-chemistry (49). The DNA strand is 20 nucleotides long from Integrated DNA technologies, including a 14-poly-T tether followed by a 6-nucleotide "sticky end" that can hybridize with complimentary strands on the substrate. The brush-mediated DNA functionalization results in a high-density DNA coating of about 0.1 nm^{-2}. We can vary the fraction of strands with sticky ends on the brush from 5% to 100%. Here, we show results for 5% sticky ends. Still, we find qualitatively similar results for all other sticky fractions explored, corresponding to a range of working temperatures 25 to 65 °C (*SI Appendix*, section 6). The particles are sufficiently light that gravity does not affect their binding properties (48) (*SI Appendix*, section 1.5). At each temperature, particles are tracked for about 20 min at $\Delta t = 0.2$ s intervals. Images are then analyzed using the TrackPy software to obtain the time evolution of individual particle positions $x(t)$ and $y(t)$ along the surface (50). We perform trajectory analysis in such a way as to avoid biases from excursions in the vertical direction (*SI Appendix*, section 1.3).

A single particle already demonstrates two types of mobility. Fig. 1*B* shows a time series of the magnitude of the displacement, $\Delta r = \sqrt{\Delta x^2 + \Delta y^2}$, where Δx, Δy are horizontal displacements undergone by the particle in between each frame. The particle alternates between taking many short steps, punctuated by bursts of longer steps. A histogram of step sizes Δx, representing both the horizontal Δx and vertical Δy increments of a particle's trajectory, is distinctly non-Gaussian (Fig. 1*C*), with a sharp kink at the transition to a heavier-tailed region. We use this kink to define a step-size cutoff distinguishing short and long steps—which determines the placement of the dashed pink line in Fig. 1 *B* and *C*—and then color the particle's 2D trajectory (Fig. 1*D*) according to whether the steps are short (orange) or long (blue). This gives another picture of the particle's motion, showing that short steps correspond to motion that is fairly localized, where exploration is limited—which we refer to as crawling—whereas long steps allow the particle to move to farther regions—which we refer to as hopping. These two modes of motion occur everywhere on the sample and can be observed repeatedly for particles whose trajectories are long enough (*SI Appendix*, section 2).

Diffusion, Crawling, and Hopping Properties Depend on Temperature. To gain more insight into the particles' mobility, we investigate the motion of the particles at different temperatures. The fraction of unbound particles p_{unbound}, which we define by the number of particles that go out of focus for at least 1 min, increases sharply around a critical temperature T_m, the melting

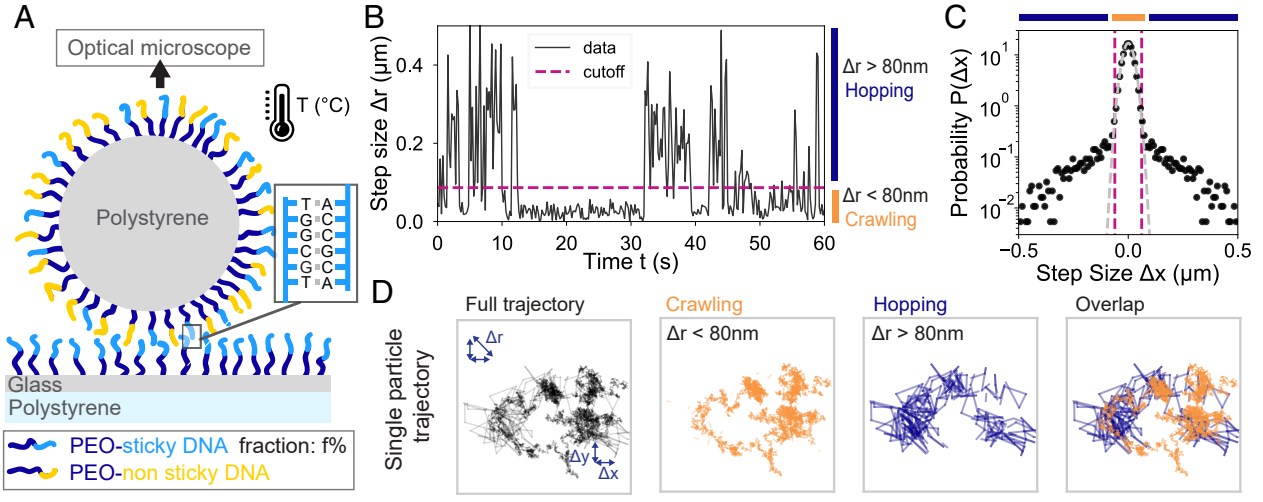

Fig. 1. Intermittent hopping and crawling of a single DNA-coated colloid. (*A*) Experimental setup. 1 μm-diameter polystyrene particles coated with DNA strands bind to and diffuse on a glass surface covered with complementary DNA. Their motion is tracked with an optical microscope. We tune the system's temperature and the fraction of sticky DNA on the particle. (*B*) Time series of step sizes for a single particle with $f = 5\%$ sticky ends around its melting temperature, at $T = 38.2$ °C and (*C*) step size distribution over the entire particle's trajectory. (*D*) Trajectory of (*B*), in black, colored, from *Left* to *Right*, as only steps smaller (orange) or larger (blue) than 80 nm, and overlap. The trajectory displayed is 15 min long and the box size is 2.8 μm.

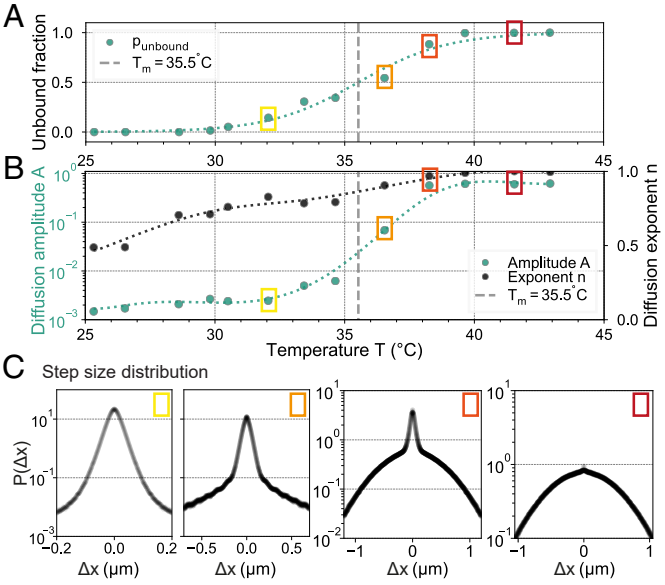

Fig. 2. Step properties change drastically with temperature. (*A*) Fraction of unbound particles with $f = 5\%$ sticky ends as in Fig. 1. (*B*) Diffusion amplitude *A* (green) characterizing the slow-down with temperature and diffusion exponent *n* (gray, *Right* axis). Dotted lines in (*A* and *B*) are guides to the eye. (*C*) Step size distribution over about 800 particle trajectories at increasing temperatures ($T = 32.1, 36.5, 38.3, 41.5\,^{\circ}C$) marked by the colored boxes (yellow to red). The 2 *Left*-ward plots share the same vertical axis.

temperature (9) (Fig. 2*A*). We also measure the mean-squared displacement $\langle r^2(t)\rangle$ at each temperature, averaging over all particles and over each trajectory. We then fit the data, using a standard least-squares procedure, as $\langle r^2(t)\rangle = 4AD_0t_0(t/t_0)^n$. Here, $D_0 = k_BT/6\pi\eta R \simeq 1\ \mu m^2/s$ is the bulk diffusion coefficient of the particle (with k_BT the thermal energy, R the particle radius, and η the fluid viscosity), $t_0 = R^2/4D_0 \simeq 63$ ms is the time for the particle to diffuse its diameter, and we fit for A and n (Fig. 2*B*).

The particle's motion is diffusive ($n \simeq 1$) at high temperatures, with a diffusion amplitude $A \simeq 0.5$, corresponding to increased hydrodynamic friction near the substrate (51, 52). Since the depth of focus is roughly the size of the particles ~560 nm, we may estimate that imaged particles are 10 to 50 nm from the surface. Such distances yield a hydrodynamic diffusion amplitude A that varies only weakly with distance to the surface (51–53). Using the logarithmic scaling law in ref. 51 gives that $A^{(th)} \simeq 0.53$ to 0.67, where the superscript $^{(th)}$ indicates theory predictions, and is close to the experimental value.

As the temperature decreases, motion progressively becomes subdiffusive ($n < 1$), especially at low temperatures $T \simeq T_m - 10\,^{\circ}C$ where $n \simeq 0.5$. This property was already highlighted in previous work (28, 30). Concomitantly, the diffusion amplitude radically slows down around the melting temperature, where A decreases by about 3 orders of magnitude. Our goal is to understand how the 2 microscopic modes of motion are related to this dramatic macroscopic decrease in diffusion amplitude and the subdiffusive behavior.

The step size distribution $P(\Delta x)$ of all particles drastically changes with temperature (Fig. 2*C*). At high temperatures, when particles are unbound, the distribution is close to a single Gaussian distribution (Fig. 2 *C*, *Right*, red box). At a slightly lower temperature (Fig. 2 *C*, *Right*, orange box) a central peak emerges in the step size distribution, an indicator of dual-mobility. As temperature decreases further, this peak becomes predominant (Fig. 2 *C*, *Left*, orange, and yellow boxes). The temperature dependence of the distribution rules out that non-Gaussianity could be caused by local hydrodynamic friction close to the surface (53–55). The non-Gaussian distributions may therefore be attributed to multiple mobility modes (33).

To unravel the temperature-dependent properties of each mode, we fit the step size distributions with a sum of 2 zero-mean Gaussians with different widths (Fig. 3*A*),

$$P(\Delta x) = \frac{p_{hop}}{\sqrt{2\pi\sigma_{hop}^2}}\exp\left(-\frac{\Delta x^2}{2\sigma_{hop}^2}\right) + \frac{p_{crawl}}{\sqrt{2\pi\sigma_{crawl}^2}}\exp\left(-\frac{\Delta x^2}{2\sigma_{crawl}^2}\right). \quad [1]$$

The parameters have a natural interpretation: $p_{hop} = 1 - p_{crawl}$ is the probability to hop and p_{crawl} the probability to crawl; σ_{crawl} and σ_{hop} are the characteristic step sizes in each mode. We use a least-squares procedure to fit p_{hop}, σ_{hop}, and σ_{crawl}. The Akaike information criterion (AIC) quantifies the relative likelihood that this fit is representative of the data (56). The AIC for this 2-Gaussian fit is much smaller than that for a 1-Gaussian fit at low temperatures (Fig. 3*B*), indicating that 2 Gaussians provide a better characterization. Adding a third Gaussian increases the AIC, confirming that the 2-Gaussian fit is the most informative model and that using 3 Gaussians would be overfitting. At high temperatures, the step size distributions approach a single Gaussian, consistent with the expectation that at these temperatures, colloids should move freely. We report in *SI Appendix*, section 3 further details on the fitting procedure, and find the parameters we obtain are only marginally sensitive to the fitting method.

The extracted probabilities to be in either mode, p_{hop} or p_{crawl}, depend strongly on temperature (Fig. 3 *C*, *i*). These probabilities undergo a sharp transition a few degrees above T_m, with crawling (or hopping) being more likely below (or above) T_m. This can be understood in the light of the melting curve in Fig. 2*A*. At low temperatures, ligands are more likely to form bonds with the surface receptors, thereby slowing the particles' motion. We further observe that both characteristic step sizes σ_{hop} and σ_{crawl} decrease as temperature is lowered (Fig. 3 *C*, *ii*). This is again consistent with the melting curve of Fig. 2*A*, since at lower temperatures, we expect more ligand–receptor bonds, further inhibiting motion.

Which mode contributes the most to the particles' overall mobility? The mean squared displacement in one time step according to our fitting model is $\langle\Delta x^2\rangle = p_{crawl}\sigma_{crawl}^2 + p_{hop}\sigma_{hop}^2$. Therefore, we may define $\Delta x_{crawl} = \sqrt{p_{crawl}}\sigma_{crawl}$ and $\Delta x_{hop} = \sqrt{p_{hop}}\sigma_{hop}$ to be the effective distance covered by either crawling or hopping in one step. Even though hopping steps are longer than crawling ones, $\sigma_{hop} \gg \sigma_{crawl}$, a particle can still cover more territory by crawling if the probability to hop p_{hop} is small. We find crawling is slightly more efficient at low temperatures, $\Delta x_{crawl} \gtrsim \Delta x_{hop}$, whereas hopping is more efficient above the melting temperature, $\Delta x_{hop} \gg \Delta x_{crawl}$ (Fig. 3 *C*, *iii*).

Transport by Crawling Is More Efficient at Low Temperatures. We rationalize our observations using a previously introduced model of DNA-coated colloid motion (37), recalling the main ingredients here, with details provided in *SI Appendix*, section 4. First, we determine the number of interacting strands N and the average number of bonds $\bar{N}_b$ with temperature, accounting

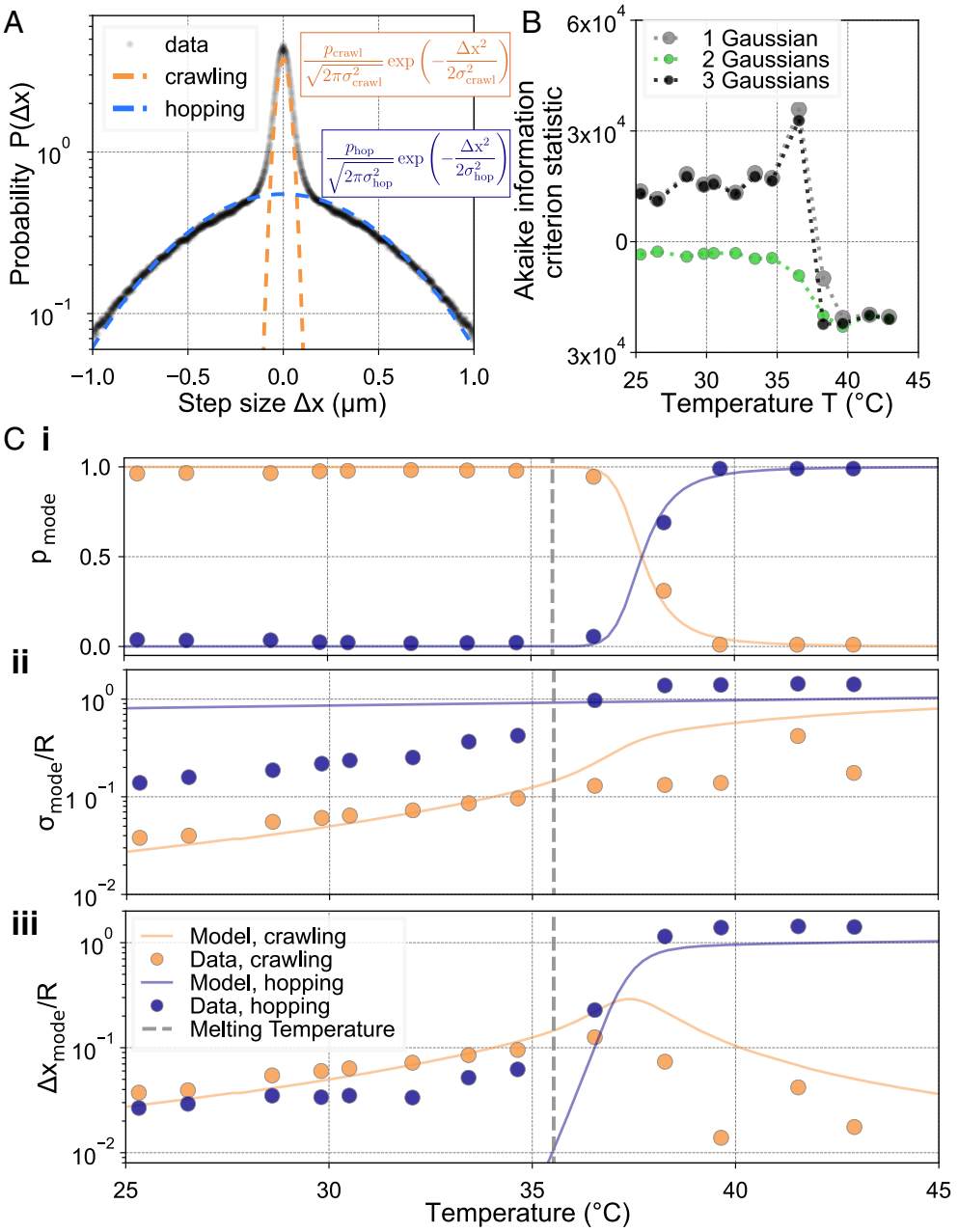

Fig. 3. Various modes of motion according to temperature. (*A*) Example of 2-Gaussians fit procedure on a representative dataset for $f = 5\%$ sticky ends at $T = 38.3$ °C; see more examples in *SI Appendix*, section 3. (*B*) Akaike information criterion for the 1, 2, or 3-Gaussians fitting procedure with temperature for $f = 5\%$ sticky ends. (*C*) Extracted fitted parameters, from *Top* to *Bottom*: (*i*) probability, (*ii*) typical step size, and (*iii*) effective distance covered in either mode; with temperature for $f = 5\%$ sticky ends. The legend and the horizontal axis are common to (*i–iii*). *SI Appendix*, Fig. S12 reports (*i*) in log-scale on the vertical-axis.

for steric and hybridization interactions (41, 48, 57). We then add kinetics by assuming DNA strands perform a random walk constrained by a harmonic spring force with spring constant k based on a worm-like chain model for the polymers (37). Strands bind and unbind independently with rates q_{on} and q_{off} respectively (37), which are related via the average number of bound strands $\bar{N}_b = N\frac{q_{\text{on}}}{q_{\text{on}}+q_{\text{off}}}$. At a given time t, $N_b(t)$ strands are bound and exert recoil forces on the particle giving an equation of motion for the particle, in the x direction

$$\frac{\mathrm{d}x(t)}{\mathrm{d}t} = \sum_{i=1}^{N_b(t)} \frac{k}{\Gamma + N_b(t)\gamma} l_i + \sqrt{\frac{2k_BT}{\Gamma + N_b(t)\gamma}}\eta(t), \quad [2]$$

where l_i is the extension of the ith strand in the x direction, $\Gamma = k_BT/D_0^{\text{hydro}}$ is the friction coefficient on the particle with $D_0^{\text{hydro}} = D_0A^{(th)}$ the diffusion coefficient of the unbound particle, accounting for hydrodynamic friction in the vicinity of a plane (51), γ the friction coefficient on each strand, and $\eta(t)$ is Gaussian white noise. Motion in the y direction is similar. We model dynamics in the z direction with simplifying arguments, assuming particles switch between 2 states: in the binding region or not. In each state, the diffusion coefficient is the same, and the switching rates depend on the particle's buoyancy. When the particle is out of the binding region, strands can not bind. Coarse-graining over the fast strand motion and binding kinetics, we obtain an analytic expression for the effective diffusion coefficient of the particle as a function of the microscopic DNA (N, q_{on},

q_{off}, k, and γ) and particle parameters (Γ). All these parameters are known from experimental data, except the density of strands on the glass surfaces, which is fitted once to obtain the correct melting temperature and is comparable (0.009 nm^{-2}) with previous work (37, 48).

Within our model, the probability of hopping is the equilibrium probability that no bonds are formed,

$$p_{\text{hop}}^{(\text{th})} = \left(\frac{q_{\text{off}}}{q_{\text{off}} + q_{\text{on}}}\right)^N, \quad p_{\text{crawl}}^{(\text{th})} = 1 - p_{\text{hop}}^{(\text{th})}. \qquad [3]$$

The probability to hop p_{hop} depends on T, since as temperature decreases, the DNA hybridization energy decreases (57) so that q_{off} should decrease. We expect q_{on} to be roughly constant with temperature (58). The mean step size in each mode is obtained by assuming that motion is Brownian (steps are Gaussian and uncorrelated), so that $(\sigma_{\text{mode}}^{(\text{th})})^2 = 2D_{\text{mode}}^{(\text{th})}\Delta t$, where $D_{\text{mode}}^{(\text{th})}$ are the diffusion coefficients associated with each mode, given by our theory (37) as

$$D_{\text{hop}}^{(\text{th})} = D_0^{\text{hydro}}, \quad D_{\text{crawl}}^{(\text{th})} \underset{N \gg 1}{\simeq} \frac{D_0^{\text{hydro}}}{1 + \bar{N}_b \frac{k}{q_{\text{off}}} \frac{k_B T}{D_0^{\text{hydro}}}}. \qquad [4]$$

With this model, we obtain the effective distance covered in either mode $(\Delta x_{\text{mode}}^{(\text{th})})^2 = 2p_{\text{mode}}^{(\text{th})} D_{\text{mode}}^{(\text{th})} \Delta t$.

At low temperatures, we expect the number of interacting strands to be large, $N \gg 1$. The distance covered in each mode then decays as $\Delta x_{\text{crawl}}^{(\text{th})} \sim 1/\sqrt{N}$ and $\Delta x_{\text{hop}}^{(\text{th})} \sim \exp(-N)$, demonstrating that $\Delta x_{\text{crawl}}^{(\text{th})} \gg \Delta x_{\text{hop}}^{(\text{th})}$ when $N \gg 1$ at low temperatures. Hopping requires all bonds to detach from the surface, which is unlikely when the number of bonds is large, making crawling a more efficient mode of transport at low temperatures.

Microscopic Mechanisms Underlying the Mode of Transport: Model and Experiment. We start by analyzing the similarities between the model (lines in Fig. 3*C*) and experiment (markers). The model captures p_{hop} and p_{crawl} around the melting temperature remarkably well, and thus the transition between hopping and crawling (Fig. 3 *C*, *i*), supporting our hypothesis that hopping arises when all bonds simultaneously detach. The effective step sizes for crawling, σ_{crawl}, $\sigma_{\text{crawl}}^{(\text{th})}$ agree well for $T < T_m$, both decreasing with temperature (orange in Fig. 3 *C*, *ii*). The measured and predicted effective distance covered in Fig. 3 *C*, *iii* agree when both the step size and probability agree. The decrease in the theoretical step size for crawling arises because the average number of bonds $\bar{N}_b$ increases, which increases the effective friction on the particle (Eq. **4**). An increase in the number of bonds is thus a potential mechanism for the increasingly shorter steps at low temperatures.

The temperature at which the two modes are equally efficient, both experimentally and theoretically, occurs slightly above the melting temperature and also corresponds to a maximum in the effective distance covered by crawling. The maximum corresponds to a trade-off between more probable crawling events and smaller crawling steps with decreasing temperatures. The optimal crawling speed in our model corresponds roughly with $N_b \simeq 4$ bonds (note that $N_b(T_m) = 9$). A similar trade-off was predicted in a simulation of particles in concentration gradients (59) and the optimal bond number was around $N_b \simeq 5$.

Discrepancies between theory and data also shed further insight into the dual hopping-crawling motion. For $T > T_m$, the theory overpredicts the measured steps, $\sigma_{\text{crawl}}^{(\text{th})} > \sigma_{\text{crawl}}$. We speculate that crawling steps may be dominated by outlier particles with a slightly higher local ligand or receptor density. These are not accounted for in our mean-field model, and such corrections of the model are also needed to explain a broader experimental melting curve than predicted by the theory (*SI Appendix*, section 4.2). The effective step sizes for hopping, σ_{hop} and $\sigma_{\text{hop}}^{(\text{th})}$ (blue), agree within 15% at high temperatures, $T > T_m$, with a slight mismatch possibly attributable to variability in the exact particle size or density, with slightly smaller particles diffusing faster and lighter ones further away from the surface having less hydrodynamic friction (48).

At low temperatures, $T < T_m$, the model overpredicts σ_{hop} by a factor of 2 to 10. Several sensible arguments for this discrepancy can be called forth, each yielding small corrections. First, the increased hydrodynamic friction from the soft polymer mesh (60, 61) could reduce $\sigma_{\text{hop}}^{(\text{th})}$. Using Brinkman lengths and polymer brush thicknesses obtained σ_{hop} in a previous work (48), we find this amounts to decreasing σ_{hop} by only a factor 2. Second, the subdiffusive motion for low temperatures mildly reduces the actual displacement as $\sigma_{\text{hop}}^{(\text{n,th})} = \sigma_{\text{hop}}^{(\text{th})} (\Delta t/t_0)^{(n-1)/2} \simeq 0.7\sigma_{\text{hop}}^{(\text{th})}$, where $n \simeq 0.5$ is the experimentally measured subdiffusive exponent in Fig. 2*B*. Another source of slight underestimation of σ_{hop} comes from fitting the wings of the distribution, which the fitting procedure tends to underestimate (*SI Appendix*, section 3). The remaining factor is that our experiments are too slow to resolve the different transport modes at low temperatures. Hence, the hopping measurements are actually a mix of hopping and crawling steps. We will explore this possibility next.

Crawling and Hopping Durations Are Diverging and Power-Law Distributed. To investigate whether we can temporally resolve the different transport modes at all temperatures, we extracted the durations of crawling and hopping events from our data, τ_{crawl}, τ_{hop}, by determining a step size cutoff from the intersection point between the 2-Gaussian fit at each temperature (Fig. 4*A*). The average duration of each mode, $\langle\tau_{\text{crawl}}\rangle$ and $\langle\tau_{\text{hop}}\rangle$, dramatically changes with temperature (Fig. 4*B*). Crawling phases last about $\langle\tau_{\text{crawl}}\rangle \simeq 5$ s at low temperatures but are much shorter at high temperatures, $\langle\tau_{\text{crawl}}\rangle \simeq \Delta t$. In contrast, hopping phases are short at low temperatures, $\langle\tau_{\text{hop}}\rangle \simeq \Delta t$, but longer at high temperatures, $\langle\tau_{\text{hop}}\rangle \simeq 5$ s. These observations suggest that we are not fully resolving hopping phases at low temperatures and crawling phases at high temperatures.

Steps that we identify as "hopping" at low temperatures may contain a mixture of hopping and crawling motions, making the measured step size smaller than it would otherwise be. This is consistent with our theoretical model since the model overestimated hopping step sizes at low temperatures. It is also consistent with *SI Appendix*, Fig. S12 showing probabilities of either mode in log scale (Fig. 3 *C*, *iii* in log scale), where we find experimental probabilities to hop are higher than in the model. Similarly, steps that we identify as "crawling" at high temperatures also contain some hopping, making them longer than they otherwise would be. Yet, at high temperatures, the model overestimated crawling step sizes. Differences between the

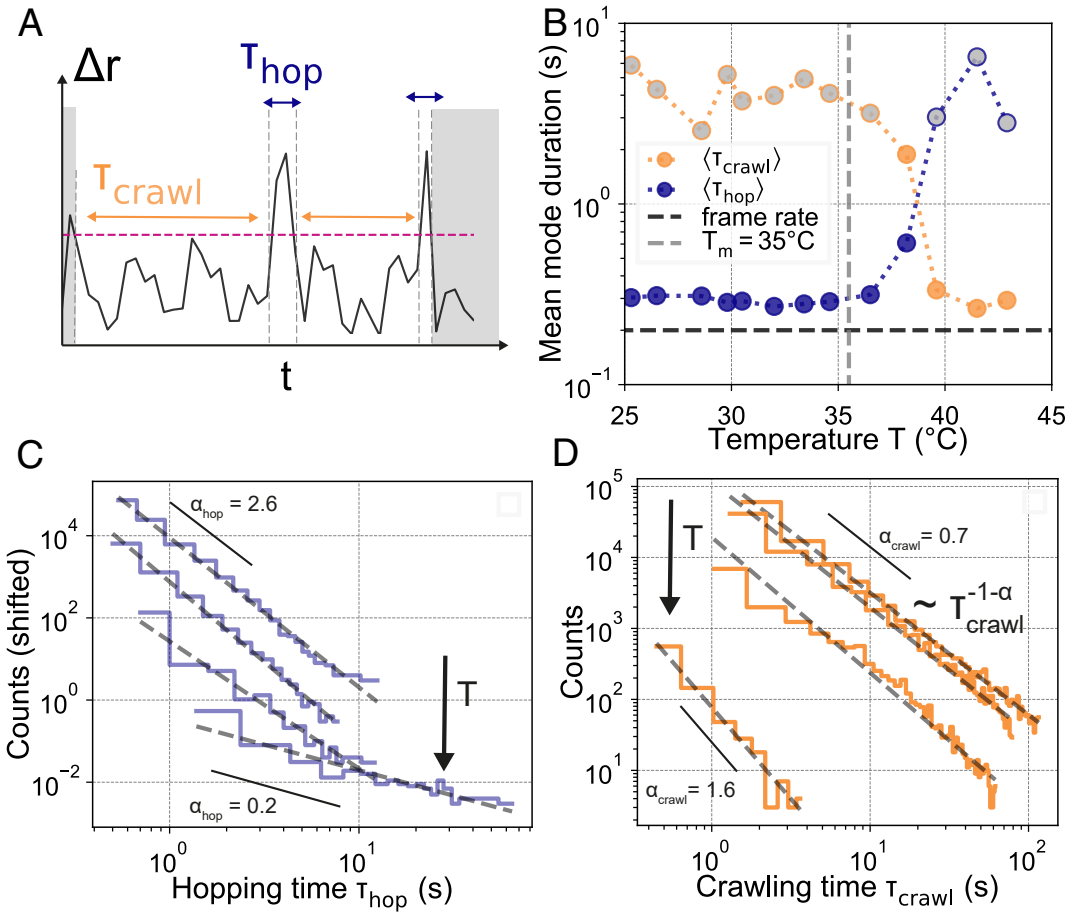

Fig. 4. Slow random switches between the 2 mobility modes. (*A*) Schematic illustrating the duration of hopping and crawling phases (*B*) Mean mode duration with temperature as obtained from averaging experimental data; notice the log scale on the vertical-axis. (*C*) Distributions of hopping and (*D*) crawling mode durations. The dashed lines are power-law fits as $\tau^{-1-\alpha}$. Gray points in (*B*) correspond to points where the average is ill-defined since $\alpha < 1$. In (*C* and *D*) $T = 25.3, 32, 36.5, 39.6$ °C, with increasing temperatures presented from *Top* to *Bottom*. In (*C*) only, each curve is displaced by a factor 10 to enhance visibility, with the highest curve having actual units. $f = 5\%$ sticky ends on the particle.

model and experiments at high temperatures may be dominated by outlier particles with a higher ligand or receptor density.

The distributions of durations can be accounted for with power laws as $p(\tau_{\text{mode}}) \simeq \tau_{\text{mode}}^{-1-\alpha_{\text{mode}}}$ (Fig. 4 *C* and *D*), at all temperatures (*SI Appendix*, section 5.1). The power-law scaling is a sign of non-Markovian dynamics, or memory, since switching times should be exponentially distributed in a Markovian process. Previous work has also observed similar power laws in the distribution of times that particles appeared to be bound—which can be compared to our crawling times (14, 28, 62). Here, we show in addition that this is true also for the hopping times.

The exponent of the power law α_{mode} depends on the mode and on temperature T. For hopping steps, we find $\alpha_{\text{hop}} \simeq 2-3$ at low temperatures while $\alpha_{\text{hop}} \simeq 0.2$ at high temperatures. In contrast, for crawling steps, $\alpha_{\text{crawl}} \simeq 0.7$ to 0.9 at low temperatures and increases at high temperatures up to $\alpha_{\text{crawl}} \simeq 1.5$ to 2. When $\alpha < 1$, the power law distribution predicts that the mean duration of a mode diverges $\langle\tau_{\text{mode}}\rangle = \infty$, since $\int_0^\infty t(t^{-1-\alpha})\mathrm{d}t$ diverges. We highlight the temperature points where $\alpha_{\text{mode}} < 1$ as gray dots in Fig. 4*B*, indicating that experimental estimates of $\langle\tau_{\text{mode}}\rangle$ are likely inaccurate for these points. In practice, the duration of a mode may still be finite since long tails, including for DNA-coated colloid binding, can have exponential decays in the very long range (14, 62). Overall, the particles thus spend extremely long times in the crawling or hopping modes at low or high temperatures, respectively.

Anticorrelation between Subsequent Steps Is Related to Subdiffusion. How are these slow switching times connected to subdiffusion? To understand subdiffusion, we must go beyond our microscopic model (Eqs. **3** and **4**) since it can only predict diffusive motion. To do so, we will simply compare our dataset with established classes of coarse-grained subdiffusive random walks, here, continuous time random walks (CTRW), confined CTRW (CCTRW), and fractional Brownian walks (FBM) (63). Briefly, CTRW is a generalization of a random walk where the wandering particle waits for a random time between jumps—which captures to some extent the waiting between hopping events. The confined CTRW is a CTRW with spatially bounded jumps—which could capture the presence of heterogeneities in binding affinities on the substrate. FBM is a generalization of a random walk where the wandering particle jumps with noisy increments with long-ranged time correlations—which could capture heterogeneities or slow binding/unbinding dynamics of multiple tethers. Rather than giving us a microscopic understanding, since none of these frameworks can capture the presence of 2 mobile modes, these mathematical concepts will give us a macroscopic insight into the subdiffusive phenomena at play.

A previous investigation of only-hopping DNA-coated colloids (28) highlighted that subdiffusion could be explained within the framework of CTRW, where the random time intervals are sampled from the power-law distributions of hopping times. This is deceptively supported by the fact that the measured exponent

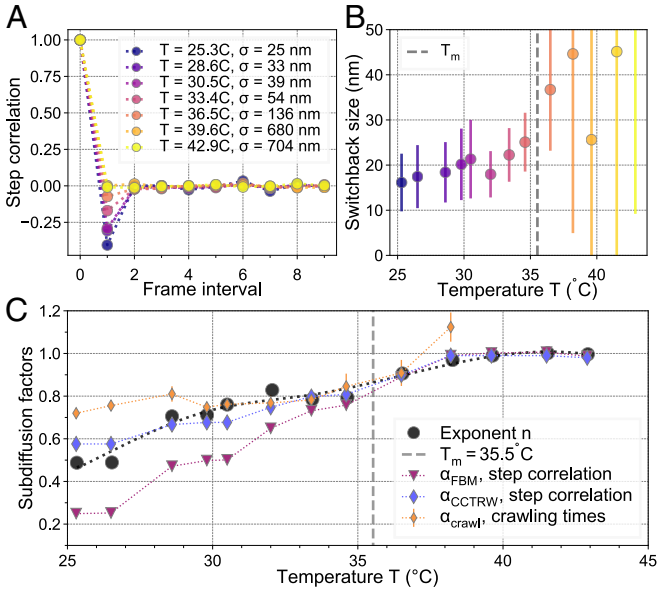

Fig. 5. Subdiffusion explained by non-Markovian switchbacks. (*A*) Step correlation as a function of the interval $\Delta\tau$ between frames at different temperatures. The step correlation is normalized by that when $\Delta\tau = 0$. Captions indicate the mean step size $\sigma = \sqrt{\langle \Delta x^2 \rangle}$. (*B*) Switchback step size defined from the magnitude of the anticorrelation peak, $\sqrt{2\langle \Delta x(t)\Delta x(t+\Delta t)\rangle}$ (*A*) with temperature. Error bars correspond to the SEM. (*C*) Subdiffusion factors obtained from fitting the switchback dynamics or from time distributions of Fig. 4; see text for details, compared to the subdiffusion exponent *n*. Dotted lines are guides for the eyes. The data for α_{crawl} only goes up until $T = 38.2\,^{\circ}\text{C}$ since beyond that point, data are not statistically relevant to fit power law distributions.

characterizing subdiffusion n, as $\langle r^2(t)\rangle \sim t^n$, (Fig. 5*C*, black) appears to be in close agreement, at least for $T \gtrsim 30$ °C, with the exponent for the power law distributions $n \simeq \alpha_{\text{crawl}}$ (orange diamonds). However, we could find no explanation for this fortuitous agreement. In fact, for CTRW, the mean-squared displacement, averaged over particles and time windows (as is done here, and in ref. 28), scales linearly as $\langle r^2(t)\rangle \sim t$. It is a common misconception that CTRW should result in subdiffusion (63–66).

To unravel the mechanism yielding subdiffusion in our colloids, we calculate the velocity step correlation as $\langle \Delta x(t)\Delta x(t+\Delta\tau)\rangle$ with a variable time $\Delta\tau$ in between steps and $\Delta x(t) = x(t+\Delta t) - x(t)$ the step size between 2 consecutive frames (Fig. 5*A*). Since it is hard to disentangle crawling and hopping at some temperatures, we combine all modes for this analysis. At low temperatures, we find the steps are anticorrelated. The magnitude of the anticorrelation increases with decreasing temperatures. If the interval n_f between frames is increased, taking $\Delta x_{n_f}(t) = x(t+n_f\Delta t) - x(t)$ with $n_f = 1, 2, \ldots 10$, then the magnitude of the anticorrelation peak $\langle \Delta x_{n_f}(t)\Delta x_{n_f}(t+\Delta t)$ consistently decreases (*SI Appendix*, Fig. S16). Such a signature of non-Markovianity, or memory, is quite visible even at the single particle level (*SI Appendix*, Fig. S16*A*) and corresponds, visually, to switchbacks in trajectories, with traces remaining in confined patches (Fig. 1*D*).

An anticorrelated velocity is reminiscent of both FBM and CCTRW (63). Anticorrelation peaks, in contrast, do not appear in CTRW (63). Both coarse-grained formalisms of FBM and CCTRW allow one to extract a variable α_{Walk} from the relative magnitude of the anticorrelation peak. α_{Walk} characterizes the random walk and results in subdiffusion as $\langle r^2(t)\rangle \sim t^{\alpha_{\text{Walk}}}$. We find remarkable agreement between α_{CCTRW} (blue diamonds) and the subdiffusive exponent n (black dots), at all temperatures, and a mild agreement between α_{FBM} (Fig. 5*C*, purple triangles) and n. In another dataset with a sticky fraction $f = 100\%$, we find that FBM agrees better with n than CCTRW. Whether a FBM or a CCTRW better describes our system requires further analysis such as ergodicity or asphericity measurements (64, 65), unfortunately only accessible for much longer datasets than ours. It is also a rather vain attempt since these macroscopic walks cannot describe our systems well as they do not produce two mobility modes. Rather, this suggests a key feature of this subdiffusive process which any model must explain is the anticorrelated steps.

Why do these switchbacks occur? The absolute value of the switchback step size, shown in Fig. 5*B*, is about 20 nm for temperatures below the melting temperature. Above the melting temperature, the switchbacks are rare events and it is not possible to estimate their size accurately. The typical extension of the PEO-DNA brushes, $\ell \sim \sqrt{k_B T/k} \simeq 5$ nm, where $k \simeq 0.16\,\text{mN.m}^{-1}$ (37), is insufficient to explain the switchbacks via a recoil effect. The system is completely overdamped, which rules out inertial effects (67). The emergence of non-Markovianity in this system is, therefore, entirely surprising. As a possible explanation for subdiffusion, the visual link between switchbacks and patchy trajectories in space points, nonetheless, to substrate heterogeneity. Dense patches of sticky DNA could be a source of "energetic confinement," reflecting the CCTRW, making it harder to escape dense sticky patches where the particle's energy is lower, resulting in switchbacks. Another possible explanation could lie in the rocking motion of the colloids. Such motion around a fixed tethering point would appear like a confined translational motion. A 20 nm displacement would amount to a 0.04 rad = 2° rocking angle. If the patch of tethered DNA is about 10% of the colloid's size, this stretches a tether by $0.1 \times R \times 0.04 \simeq 2$ nm which is reasonable compared to entropic stretching $\ell \simeq 5$ nm.

Discussion

In summary, we have observed 2 simultaneous, randomly alternating mobility modes for micron-sized DNA-coated colloids: hopping, corresponding to fast and long steps, that dominates at temperatures above the melting temperature T_m; and crawling with slow and short steps that dominates below T_m. Both hopping and crawling occur at the single and ensemble particle level: Particles rapidly switch between the 2 modes, with power-law distributed switching times. Within our theoretical model that captures the main features of the experiments, we interpret that hopping corresponds to events where a particle detaches all bonds from the surface, floats in free space, and reattaches. Crawling is a cohesive move on the surface, where the particle is always in contact through a few bonds. Crawling slows down with decreasing temperatures as more bonds form and exert recoil forces, explaining the strong mobility slowdown by orders of magnitude. At low temperatures, switchbacks in the trajectory become increasingly present, highlighting the emergence of memory and consistent with the particles' subdiffusive motion. We hypothesize that these switchbacks originate from heterogeneous coating densities on the substrate or rocking motion.

Our analysis sheds light on seemingly disparate mobility results in the literature (28, 30). In fact, the DNA-coated colloids in ref. 28 were likely only observed to hop because the coatings were low density, preventing strands from extending in a coordinated fashion to crawl. Since the effective distance covered by hopping

decays even faster with cooling than crawling, this explains the extremely fast slowdown of transport for the colloids in ref. 28. In contrast, the DNA-coated colloids in ref. 30 were only observed to perform cohesive motion at low temperatures. Since they are densely coated, similar to ours, and were only investigated below the melting temperature, our analysis shows that cohesive motion (crawling) is predominant. We find that both hopping and crawling occur for DNA-coated colloids with sufficiently dense coatings.

Clearly, high-density coatings can increase a particle's mobility at low temperatures as they enable particles to crawl while remaining attached. Remarkably, colloids with a higher fraction of sticky ends crawl with a ~50% probability even at high temperatures (*SI Appendix*, section 6), although transport by crawling is not as efficient to cover large distances as hopping at these higher temperatures. Our analysis thus shows, through the mechanism of crawling, why high-density colloids result in improved self-assembly (14, 19, 20, 23, 48).

While our experiments and model provide valuable insights into transport in ligand–receptor systems, they also raise a number of questions and open broad avenues of inquiry. Thus, to make further progress, we propose the following road map for future investigations.

On the experimental side:

- acquire images with a refined time step to resolve each mode accurately ($\Delta t \ll 0.2$ s);
- investigate long trajectories to assess particle-to-particle variability;
- track the 3D motion of particles to investigate the link between lateral mobility and excursions far from the surface;
- track orientational motion to resolve rolling versus sliding versus rocking dynamics in the crawling motion mode;

On the modeling side:

- design models with non-Markovian features at equilibrium, in the binding process, building on ref. 68;
- account for spatially heterogeneous binding properties, which are increasingly hypothesized to play a role in the mobility and self-assembly features (69);
- link in- and out-of-equilibrium models e.g. inspiring from refs. 35 and 70.

Our roadmap is linked with several open mechanistic questions. First, the diversity of modeling approaches, in particular in the ways binding kinetics are accounted for (26, 35, 37, 44, 59), suggests that studies that could shed light on the detailed binding kinetics are still needed. These investigations are now within reach with, for example, interferometric scattering microscopy (71). How do collective long-time memory effects emerge from single DNA strands that may, at the single DNA strand level, exhibit intermittent hopping (72)? Since our method is limited to 2D tracking, it is not possible to distinguish here between various potential crawling modes, for example, between sliding or rolling DNA-coated colloids. With the advent of 3D, superresolution microscopy as well as advanced colloidal particle designs (73–75), we may be able to distinguish these mobility modes. Furthermore, separating each mode of motion should help uncover more precisely the origin of subdiffusive motion (28), since some modes may be more prone to memory effects than others (76). Such detailed microscopic inquiries will further pave the way toward advanced and rational programming of ligand–receptor motion.

Materials and Methods

We report here only the main methods used for colloidal synthesis and tracking. Other experimental details are discussed in *SI Appendix*, section 1.

DNA-Coated Polystyrene Colloids. DNA-coated polystyrene (PS) colloidal spheres are synthesized using the swelling/deswelling method reported in ref. 47. Polystyrene-b-poly(ethylene oxide) copolymers PS(3,800 g/mol)-b-PEO(6,500 g/mol) are purchased from Polymer Source Inc, and are first functionalized with azide at the end of the PEO chain. Then, the PS-b-PEO-N3 chains are tethered to the PS particles using the swelling/deswelling method. During the synthesis, 15 μL of 1 μm particles (10 w/v, purchased from Thermo Scientific), 125 μL deionized (DI) water, 160 μL tetrahydrofuran (THF), and 100 μL of PS-b-PEO-N3 are mixed at room temperature. The mixture is placed on a horizontal shaker (1,000 rpm) for 1.5 h to swell the PS particles fully and the PS block of the PS-b-PEO-N3 is adsorbed to the PS particle's surface. Then, THF is slowly removed from the solution via evaporation by adding DI water while leaving the hydrophobic PS blocks physically inserted into the particles and the hydrophilic PEO chains extending out into the solution. The particles are then washed with DI water 3 times to remove excess polymers. Single-stranded DNA (ssDNA, 20 bases, purchased from Integrated DNA Technologies) with 5′ dibenzocyclooctyne (DBCO) end modification, is clicked to the N3 (at the end of PS-b-PEO-N3) through strain-promoted alkyne-azide cycloaddition (49). PS particles previously coated with the PS-b-PEO-N3 polymer brush are dispersed in 200 μL of 500 mM PBS buffer, at pH 7.4. Then 10 μL of the mixed DBCO-DNA (0.1 mM) are added to the suspension. For 100% DNA, we use 10 μL 5′-/DBCO/-T14-ACCGCA-3′, and for f% DNA coverage we use a mixture of $(f/100) \times 10$ μL 5′-/DBCO/-T14-ACCGCA-3′ and $(1-f/100)$ μL of 5′-/DBCO/-T20-3′. The mixture is left to react for 48 h on a horizontal shaker (1,000 rpm). The final product is washed in DI water 3 times and stored in 140 mM PBS buffer. The DNA coverage density is measured using flow cytometry and we obtain a strand density $\sigma = (3.27\ \text{nm})^{-2}$.

DNA-Coated Glass Substrates. DNA-coated glass substrates are prepared using the same swelling/deswelling method. First, we spin coat an ultra-thin PS layer to an ultra-cleaned 22 mm × 22 mm glass coverslip (purchased from Bioscience Tools). The substrate is then swelled in the same copolymer PS(3,800 g/mol)-b-PEO(6,500 g/mol)-N3 solution in THF for 4 h on a shaking stage. Then, THF is slowly removed from the solution by adding DI and via evaporation. DNA clicking is performed in a home-made Polydimethylsiloxane (PDMS) reaction chamber for 48 h on a shaking stage, then washed 10 times in DI water to remove extra DNA. The entire sample is sealed in 140 mM PBS buffer (pH 7.4) with 0.3% w/v pluronic F127 surfactant, using Ultraviolet (UV) glue to avoid any external flow or evaporation of the buffer as we modulate the system's temperature. The DNA sequence used on the glass substrate is complementary to that on the particles, 5′-/DBCO/-T14-TGCGGT-3′. All glass substrates are coated with 100% sticky DNA 5′-/DBCO/-T14-TGCGGT-3′.

Tracking the Diffusion of DNA-Coated Colloids. To study the diffusion of DNA-coated colloids, we track the motion of about 800 particles as they bind and diffuse on the DNA-coated substrate. The sample is mounted on a lab microscope (Nikon Eclipse Ti 60X, 72 nm pixel size, depth of focus 560 nm) thermal stage with a homemade temperature controller. We keep the shutter open during the acquisition. Hematite tracer particles are embedded and fixed on the substrate and are used to substract camera drift during the tracking. Displacement measurements are performed by tracking particles over the temperature range 28 to 72 °C. At each temperature, particles are tracked over a time range of 20 min at a frame rate of 5 images per second. For the highest temperature reported here, particles diffuse faster and we only track them over 5 min. Images are then analyzed using the TrackPy software to obtain individual particle positions with time (50). Particles that do not move at all, even at high temperatures, are removed from the analysis. Such particles (less than 5%) likely have low DNA coverage or are found in a low-density DNA region where steric repulsion is not sufficient to screen van der Waals attraction, and are, therefore, stuck or "crashed" on the surface.

To avoid biases from excursions in the vertical direction, we stop trajectories when particles leave the field of view due to e.g. buoyancy. Our trajectories are generally sufficiently long that these effects represent only a minor fraction of the motion. At temperatures below the melting temperature, all trajectories last more than 20 frames (4 s). Above the melting temperature, only 50% of the trajectories last more than 20 frames (for colloids with a fraction of sticky ends of 5%). In mode duration analysis we remove the beginning and the end of the trajectory so that our analysis is not biased by these excursions.

Data, Materials, and Software Availability. Integration codes used to generate model curves are published (77). Original trajectories of 5% DNA-coated colloids at the different temperatures investigated are available in ref. 78.

ACKNOWLEDGMENTS. We acknowledge fruitful discussions with Fan Cui, Florian Rehfeldt, and Matthias Weiss. J.A.Z. and D.J.P. were supported by the US Department of Energy under grant DE-SC0007991 for the design and implementation of the experiments. M.H.-C. acknowledges support from the Alfred P. Sloan Foundation, and from the Natural Sciences and Engineering Research Council of Canada, RGPIN-2023-04449/Cette recherche a été financée par le Conseil de recherches en sciences naturelles et en génie du Canada. S.M. received funding from the European Union's Horizon 2020 research and innovation program under the Marie Skłodowska-Curie grant agreement 839225, Molecular Control.

Author affiliations: [a]Department of Physics, New York University, New York, NY 10003; [b]Department of Mathematics, University of British Columbia, Vancouver, BC V6T 1Z2, Canada; [c]Department of Chemical and Biomolecular Engineering, New York University, New York, NY 11201; [d]Department of Mathematics, Courant Institute of Mathematical Sciences, New York University, New York, NY 10012; and [e]Department of Chemistry, CNRS, Sorbonne Université, Physicochimie des Electrolytes et Nanosystèmes Interfaciaux, Paris F-75005, France

1. T. Curk, J. Dobnikar, D. Frenkel, Optimal multivalent targeting of membranes with many distinct receptors. *Proc. Natl. Acad. Sci. U.S.A.* **114**, 7210 (2017).
2. C. Boitard, A. Bée, C. Ménager, N. Griffete, Magnetic protein imprinted polymers: A review. *J. Mater. Chem. B* **6**, 1563 (2018).
3. H. T. Phan *et al*., Bimodal brush-functionalized nanoparticles selective to receptor surface density. *Proc. Natl. Acad. Sci. U.S.A.* **120**, e2208377120 (2023).
4. M. Nerantzaki *et al*., Biotinylated magnetic molecularly imprinted polymer nanoparticles for cancer cell targeting and controlled drug delivery. *Chem. Commun.* **58**, 5642 (2022).
5. A. Kowalewski, N. R. Forde, C. S. Korosec, Multivalent diffusive transport. *J. Phys. Chem. B* **125**, 6857 (2021).
6. T. Curk *et al*., Computational design of probes to detect bacterial genomes by multivalent binding. *Proc. Natl. Acad. Sci. U.S.A.* **117**, 8719 (2020).
7. P. Xu *et al*., Whole-genome detection using multivalent DNA-coated colloids. *Proc. Natl. Acad. Sci. U.S.A.* **120**, e2305995120 (2023).
8. E. W. Gehrels, W. B. Rogers, Z. Zeravcic, V. N. Manoharan, Programming directed motion with DNA-grafted particles. *ACS Nano* **16**, 9195 (2022).
9. W. B. Rogers, W. M. Shih, V. N. Manoharan, Using DNA to program the self-assembly of colloidal nanoparticles and microparticles. *Nat. Rev. Mater.* **1**, 1 (2016).
10. D. Talbot *et al*., Adsorption of organic dyes on magnetic iron oxide nanoparticles. Part I: Mechanisms and adsorption-induced nanoparticle agglomeration. *ACS Omega* **6**, 19086 (2021).
11. C. A. Mirkin, R. L. Letsinger, R. C. Mucic, J. J. Storhoff, A DNA-based method for rationally assembling nanoparticles into macroscopic materials. *Nature* **382**, 607 (1996).
12. A. P. Alivisatos *et al*., Organization of 'nanocrystal molecules' using DNA. *Nature* **382**, 609 (1996).
13. M. He *et al*., Colloidal diamond. *Nature* **585**, 524 (2020).
14. P. L. Biancaniello, A. J. Kim, J. C. Crocker, Colloidal interactions and self-assembly using DNA hybridization. *Phys. Rev. Lett.* **94**, 058302 (2005).
15. S. Y. Park *et al*., DNA-programmable nanoparticle crystallization. *Nature* **451**, 553 (2008).
16. D. Nykypanchuk, M. M. Maye, D. Van Der Lelie, O. Gang, DNA-guided crystallization of colloidal nanoparticles. *Nature* **451**, 549 (2008).
17. R. J. Macfarlane *et al*., Nanoparticle superlattice engineering with DNA. *Science* **334**, 204 (2011).
18. W. B. Rogers, W. M. Shih, V. N. Manoharan, Using DNA to program the self-assembly of colloidal nanoparticles and microparticles. *Nat. Rev. Mater.* **1**, 16008 (2016).
19. A. J. Kim, P. L. Biancaniello, J. C. Crocker, Engineering DNA-mediated colloidal crystallization. *Langmuir* **22**, 1991 (2006).
20. A. Hensley, W. M. Jacobs, W. B. Rogers, Self-assembly of photonic crystals by controlling the nucleation and growth of DNA-coated colloids. *Proc. Natl. Acad. Sci. U.S.A.* **119**, e2114050118 (2022).
21. I. Chakraborty *et al*., Self-assembly dynamics of reconfigurable colloidal molecules. *ACS Nano* **16**, 2471 (2022).
22. A. Mcmullen, M. M. Basagoiti, Z. Zeravcic, J. Brujic, Self-assembly through programmable folding. *Nature* **610**, 502 (2022).
23. N. Geerts, E. Eiser, Flying colloidal carpets. *Soft Matter* **6**, 664 (2010).
24. M. Holmes-Cerfon, Stochastic disks that roll. *Phys. Rev. E* **94**, 052112 (2016).
25. H. Alston, T. Bertrand, Boosting macroscopic diffusion with local resetting. arXiv [Preprint] (2024). https://arxiv.org/abs/2401.12772 (Accessed 24 January 2023).
26. L. Barto š, M. Lund, R. V ácha, Enhanced diffusion through multivalency. bioRxiv [Preprint] (2023). https://doi.org/10.1101/2023.09.20.558647 (Accessed 10 October 2023).
27. S. Chatterjee, W. M. Jacobs, Multi-objective optimization for targeted self-assembly among competing polymorphs. arXiv [Preprint] (2024). https://arxiv.org/abs/2401.11234 (Accessed 20 January 2024).
28. Q. Xu, L. Feng, R. Sha, N. Seeman, P. Chaikin, Subdiffusion of a sticky particle on a surface. *Phys. Rev. Lett.* **106**, 228102 (2011).
29. T. Sakai, S. I. Nishimura, T. Naito, M. Saito, Influenza a virus hemagglutinin and neuraminidase act as novel motile machinery. *Sci. Rep.* **7**, 45043 (2017).
30. Y. Wang *et al*., Crystallization of DNA-coated colloids. *Nat. Commun.* **6**, 7253 (2015).
31. T. Sakai, H. Takagi, Y. Muraki, M. Saito, Unique directional motility of influenza c virus controlled by its filamentous morphology and short-range motions. *J. Virol.* **92**, e01522 (2018).
32. J. Lowensohn, L. Stevens, D. Goldstein, B. M. Mognetti, Sliding across a surface: Particles with fixed and mobile ligands. *J. Chem. Phys.* **156**, 164902 (2022).
33. B. Wang, J. Kuo, S. C. Bae, S. Granick, When brownian diffusion is not gaussian. *Nat. Mater.* **11**, 481 (2012).
34. P. K. Jana, B. M. Mognetti, Translational and rotational dynamics of colloidal particles interacting through reacting linkers. *Phys. Rev. E* **100**, 060601 (2019).
35. C. L. Porter, S. L. Diamond, T. Sinno, J. C. Crocker, Shear-driven rolling of DNA-adhesive microspheres. *Biophys. J.* **120**, 2102 (2021).
36. S. Merminod, J. R. Edison, H. Fang, M. F. Hagan, W. B. Rogers, Avidity and surface mobility in multivalent ligand-receptor binding. *Nanoscale* **13**, 12602 (2021).
37. S. Marbach, J. A. Zheng, M. Holmes-Cerfon, The nanocaterpillar's random walk: Diffusion with ligand-receptor contacts. *Soft Matter* **18**, 3130 (2022).
38. D. Joshi *et al*., Kinetic control of the coverage of oil droplets by DNA-functionalized colloids. *Sci. Adv.* **2**, e1600881 (2016).
39. R. W. Verweij *et al*., Conformations and diffusion of flexibly linked colloidal chains. *J. Phys. Mater.* **4**, 035002 (2021).
40. Y. Ding, J. Mittal, Insights into DNA-mediated interparticle interactions from a coarse-grained model. *J. Chem. Phys.* **141**, 11B608-1 (2014).
41. S. Angioletti-Uberti, P. Varilly, B. M. Mognetti, A. V. Tkachenko, D. Frenkel, Communication: A simple analytical formula for the free energy of ligand-receptor-mediated interactions. *J. Chem. Phys.* **138**, 01B401 (2013).
42. N. A. Licata, A. V. Tkachenko, Colloids with key-lock interactions: Nonexponential relaxation, aging, and anomalous diffusion. *Phys. Rev. E* **76**, 041405 (2007).
43. G. Mitra *et al*., A coarse-grained simulation model for colloidal self-assembly via explicit mobile binders. *Soft Matter* **19**, 4223–4236 (2023).
44. J. P. Lee-Thorp, M. Holmes-Cerfon, Modeling the relative dynamics of DNA-coated colloids. *Soft Matter* **14**, 8147 (2018).
45. J. A. Janeš *et al*., First-principle coarse-graining framework for scale-free bell-like association and dissociation rates in thermal and active systems. *Phys. Rev. X* **12**, 031030 (2022).
46. L. Li et al., Biomechanics as driver of aggregation of tethers in adherent membranes. *Soft Matter* **17**, 10101 (2021).
47. J. S. Oh, Y. Wang, D. J. Pine, G.-R. Yi, High-density PEO-b-DNA brushes on polymer particles for colloidal superstructures. *Chem. Mater.* **27**, 8337 (2015).
48. F. Cui, S. Marbach, J. A. Zheng, M. Holmes-Cerfon, D. J. Pine, Comprehensive view of microscopic interactions between DNA-coated colloids. *Nat. Commun.* **13**, 2304 (2022).
49. N. J. Agard, J. A. Prescher, C. R. Bertozzi, A strain-promoted [3 + 2] azide- alkyne cycloaddition for covalent modification of biomolecules in living systems *J. Am. Chem. Soc.* **126**, 15046 (2004).
50. J. C. Crocker, D. G. Grier, Methods of digital video microscopy for colloidal studies. *J. Colloid Interface Sci.* **179**, 298 (1996).
51. B. Sprinkle, E. B. Van Der Wee, Y. Luo, M. M. Driscoll, A. Donev, Driven dynamics in dense suspensions of microrollers. *Soft Matter* **16**, 7982 (2020).
52. A. J. Goldman, R. G. Cox, H. Brenner, Slow viscous motion of a sphere parallel to a plane wall-i motion through a quiescent fluid. *Chem. Eng. Sci.* **22**, 637 (1967).
53. M. Lavaud, T. Salez, Y. Louyer, Y. Amarouchene, Stochastic inference of surface-induced effects using brownian motion. *Phys. Rev. Res.* **3**, L032011 (2021).
54. M. Matse, M. V. Chubynsky, J. Bechhoefer, Test of the diffusing-diffusivity mechanism using near-wall colloidal dynamics. *Phys. Rev. E* **96**, 042604 (2017).
55. A. V. Chechkin, F. Seno, R. Metzler, I. M. Sokolov, Brownian yet non-gaussian diffusion: From superstatistics to subordination of diffusing diffusivities. *Phys. Rev. X* **7**, 021002 (2017).
56. J. E. Cavanaugh, A. A. Neath, The akaike information criterion: Background, derivation, properties, application, interpretation, and refinements. *Wiley Interdiscip. Rev. Comput. Stat.* **11**, e1460 (2019).
57. J. SantaLucia Jr., A unified view of polymer, dumbbell, and oligonucleotide DNA nearest-neighbor thermodynamics. *Proc. Natl. Acad. Sci. U.S.A.* **95**, 1460 (1998).
58. J. X. Zhang *et al*., Predicting DNA hybridization kinetics from sequence. *Nat. Chem.* **10**, 91 (2018).
59. F. J. Martinez-Veracoechea *et al*., Designing stimulus-sensitive colloidal walkers. *Soft Matter* **10**, 3463 (2014).
60. R. J. Hill, D. Saville, W. Russel, Electrophoresis of spherical polymer-coated colloidal particles. *J. Colloid Interface Sci.* **258**, 56 (2003).
61. V. Bertin, Y. Amarouchene, E. Raphael, T. Salez, Soft-lubrication interactions between a rigid sphere and an elastic wall. *J. Fluid Mech.* **933**, A23 (2022).
62. W. B. Rogers, T. Sinno, J. C. Crocker, Kinetics and non-exponential binding of DNA-coated colloids. *Soft Matter* **9**, 6412 (2013).
63. S. Burov, J.-H. Jeon, R. Metzler, E. Barkai, Single particle tracking in systems showing anomalous diffusion: The role of weak ergodicity breaking. *Phys. Chem. Chem. Phys.* **13**, 1800 (2011).
64. F. Rehfeldt, M. Weiss, The random walker's toolbox for analyzing single-particle tracking data. *Soft Matter* **19**, 5206–5222 (2023).
65. D. Ernst, M. Hellmann, J. K öhler, M. Weiss,, Fractional brownian motion in crowded fluids. *Soft Matter* **8**, 4886 (2012).
66. Y. He, S. Burov, R. Metzler, E. Barkai, Random time-scale invariant diffusion and transport coefficients. *Phys. Rev. Lett.* **101**, 058101 (2008).
67. S. Marbach, M. Holmes-Cerfon, Mass changes the diffusion coefficient of particles with ligand-receptor contacts in the overdamped limit. *Phys. Rev. Lett.* **129**, 048003 (2022).

68. D. S. Grebenkov, Diffusion-controlled reactions with non-Markovian binding/unbinding kinetics. *J. Chem. Phys.* **158**, 214111 (2023).
69. I. C. Jenkins, J. C. Crocker, T. Sinno, Interaction heterogeneity can favorably impact colloidal crystal nucleation. *Phys. Rev. Lett.* **119**, 178002 (2017).
70. F. Ziebert, I. M. Kulić, How influenza's spike motor works. *Phys. Rev. Lett.* **126**, 218101 (2021).
71. J. Suelzle *et al.*, Label-free imaging of DNA interactions with 2D materials. bioRxiv [Preprint] (2023). https://doi.org/10.1101/2023.07.05.547763 (Accessed 14 June 2023).
72. M. J. Skaug, J. Mabry, D. K. Schwartz, Intermittent molecular hopping at the solid-liquid interface. *Phys. Rev. Lett.* **110**, 256101 (2013).
73. P. G. Moerman, H. Fang, T. E. Videb , W. B. Rogers, R. Schulman, A simple method to reprogram the binding specificity of DNA-coated colloids that crystallize. arXiv [Preprint] (2022). https://arxiv.org/abs/2206.00952 (Accessed 2 June 2022).
74. C. S. Korosec, P. M. Curmi, H. Linke, N. R. Forde, The lawnmower. An artificial protein-based burnt-bridge molecular motor. arXiv [Preprint] (2021). https://arxiv.org/abs/2109.10293 (Accessed 11 August 2023).
75. M. Muñoz-Basagoiti, O. Rivoire, Z. Zeravcic, Catalysis from the bottom-up. arXiv [Preprint] (2022). https://arxiv.org/abs/2211.12107 (Accessed 22 November 2023).
76. D. Wang, D. K. Schwartz, Non-brownian interfacial diffusion: Flying, hopping, and crawling. *J. Phys. Chem. C* **124**, 19880 (2020).
77. S. Marbach, smarbach/DNACoatedColloidsInteractions: Release with diffusion calculations. Zenodo. https://doi.org/10.5281/zenodo.6798435. Deposited 5 July 2022.
78. S. Marbach, J. A. Zheng, D. J. Pine, Replication data for Hopping and Crawling DNA Coated Colloids. Recherche Data Gouv. https://doi.org/10.57745/OCFXY2. Deposited 19 March 2023.